Scenario-based probabilistic hazard assessment for explosive events at the San Salvador Volcanic Complex, El Salvador

Alvaro Aravena[1,2,*], Andrea Bevilacqua[3], Augusto Neri[3], Pietro Gabellini[4], Dolors Ferrés[5], Demetrio Escobar[6], Alessandro Aiuppa[7], and Raffaello Cioni[4]

[1]Facultad de Ciencias Básicas, Universidad Católica del Maule, Talca, Chile

[2]Laboratoire Magmas et Volcans, Université Clermont Auvergne, CNRS, IRD, OPGC, Clermont-Ferrand, France

[3]Istituto Nazionale di Geofisica e Vulcanologia, Sezione di Pisa, Pisa, Italy

[4]Dipartimento di Scienze della Terra, Università degli studi di Firenze, Florence, Italy

[5]Escuela Nacional de Ciencias de la Tierra, UNAM, Ciudad de México, México

[6]Dirección del Observatorio Ambiental, MARN, San Salvador, El Salvador

[7]Dipartimento di Scienze della Terra e del Mare, Università degli studi di Palermo, Palermo, Italy

*Correspondence to A. Aravena (aaravena@ucm.cl).

Highlights:

- We assess the probabilistic hazard associated with explosive volcanism at the San Salvador Volcanic Complex.
- Results show that Plinian eruptions at El Boquerón volcano can deposit thick tephra layers and PDCs in the San Salvador metropolitan area.
- The simulated sub-Plinian events highlight the seasonal influence of wind patterns in tephra dispersal.

Abstract

We present a scenario-based, probabilistic hazard assessment for the San Salvador volcanic complex (SSVC), a volcanic field located in the vicinity of San Salvador that includes the El Boquerón stratovolcano and 25 monogenetic vents. We define a set of likely eruption scenarios for tephra fallout and pyroclastic density currents (PDCs). The eruption scenarios range from violent Strombolian eruptions with a significant uncertainty in source position to sub-Plinian and Plinian activity fed from the central cone. The adopted methodology is mainly based on numerical modeling using Tephra2 (adopting the software TephraProb) to study tephra fallout and the branching box model and the branching energy cone model (adopting the programs BoxMapProb 2.0 and ECMapProb 2.0) to

describe inertial and frictional PDCs, respectively. Despite the dominant W-WSW-trending winds, numerical results show that Plinian eruptions at El Boquerón volcano are able to deposit thick tephra layers in the metropolitan area of San Salvador city, likely reaching mass loads of the order of 100 kg/m^2 (conditional probability of 50%). The simulated sub-Plinian events highlight the seasonal influence of wind patterns. In fact, the conditional probability of significant tephra sedimentation in San Salvador city is strongly reduced when eruptions occur during the rainy season. Numerical modeling of violent Strombolian eruptions is performed considering uncertainty in vent position. Results show that the conditional probability of depositing tephra mass loads higher than 10 kg/m^2 at a given point reaches a maximum value of ~7% on the NW flank of the volcano, at about 8 km from the central crater. On the other hand, very low conditional probabilities (<1%) are obtained for San Salvador city for any relevant threshold (10 kg/m^2 or more) of tephra mass load during violent Strombolian events. Regarding PDCs, results show that those produced during large-scale Plinian eruptions are able to invade significant areas of the volcano surroundings, including San Salvador city. PDCs generated from the partial collapse of a sub-Plinian eruption column exhibit maximum inundation probabilities on the N, W and S flanks of the volcano. Cerro El Picacho exerts a significant shield effect on the propagation of these PDCs, with low inundation probabilities for San Salvador city (<3%). Finally, coupling published vent opening probability maps and numerical modeling of small-scale PDCs yields maximum inundation probabilities on the NW flank of the volcano, reaching maximum conditional probabilities of the order of ~10% and values of about 5% near the village of Nuevo Sitio del Niño.

Keywords: San Salvador Volcanic Complex, probabilistic hazard assessment, energy cone, box model, branching formulation.

1. Introduction

Volcanic hazard assessment delivers key information for planners and decision makers to design effective measures for volcanic risk reduction. Assessments depend upon our understanding of the

eruptive history of the volcanic system under consideration, which allows definition of the scenarios that communities will likely face in case of volcano reawakening (e.g., Cioni et al., 2008; Neri et al., 2008; Orsi et al., 2009; Marti et al., 2012; Wright et al., 2019; Rosi et al., 2022). This information is then integrated with numerical simulations to define the expected areas impacted by future eruptions (Connor et al., 2015). Numerical modeling and statistics-based volcanic hazard assessments have been performed for a large, growing number of volcanoes, including Vesuvius (Italy; Todesco et al., 2002; Esposti Ongaro et al., 2002; 2008; Cioni et al., 2003; Macedonio et al., 2008; 2016; Doronzo et al., 2022), Campi Flegrei caldera (Italy; Costa et al., 2009; Neri et al., 2015; Bevilacqua et al., 2016; 2017a; 2022a), Etna (Italy; Barsotti et al., 2010; Del Negro et al., 2013), El Misti (Peru; Sandri et al., 2014), Long Valley volcanic region (USA, Bevilacqua et al, 2018; Rutarindwa et al., 2019), Cotopaxi (Ecuador; Pistolesi et al., 2014; Tadini et al., 2021a; 2022), Yucca Mountain (Valentine et al., 2009), Mount Pelée (Martinique; Gueugneau et al., 2020) and El Hierro (Spain; Becerril et al., 2014), among others.

In the specific case of the San Salvador volcanic complex (SSVC; Figure 1), which is the focus of this paper, a probabilistic hazard assessment is not available in the literature, although a series of studies addressing the evolution of the SSVC have been published during the last decades. Fairbrother et al. (1978) studied the evolution of El Boquerón volcano through the analysis of lava flows from a geochemical and petrological point of view. Sofield (1998) studied the stratigraphy and eruptive history of SSVC (with emphasis on flank eruptions) and quantified the eruption frequency at SSVC. Major et al. (2001) reported on the main volcanic hazards that may affect people in San Salvador. Sofield (2004) defined five eruption scenarios at SSVC including events sourced from both the central vent and the flanks, presenting hazard zonation maps for specific scenarios of central volcanism. Ferrés et al. (2011) studied the stratigraphy of the last 3,000 yr, mainly based on excavations at El Cambio archeological site, and discussed how volcanic eruptions affected prehistoric settlements. Ferrés et al. (2013) reviewed the stratigraphy and eruption history of SSVC, defined three hazard

scenarios for the central vent based on reference events involving tephra fallout, ballistic projectiles and PDCs, and presented three hazard zones based on computer simulations. Finally, Bevilacqua et al. (2021) presented thematic vent opening maps for different volcanic phenomena at the SSVC, focusing on volcanic processes whose occurrence probability is distributed over a significant portion of the volcanic field, such as lava flows, small-scale PDCs and small-scale tephra fallout (see also Bevilacqua et al. 2015; 2017b). Conversely, Bevilacqua et al. (2021) proposed that Plinian and sub-Plinian eruptions able to produce large-scale PDCs and voluminous tephra deposits are expected to be sourced with much larger probability from the central vent of the SSVC (i.e., El Boquerón volcano).

Different authors have argued on the critical importance of flank eruptions in the SSVC. This is due to the large population living on the flanks of El Boquerón volcano, the continuous growth of the city toward this zone, and the relatively frequent flank volcanic activity documented during the last 3,000 yr (Sofield, 2004; Ferrés et al., 2011). Despite this, almost all the analyses of volcanic hazard zonation at SSVC are devoted to eruptions sourced from the central cone (Sofield, 2004; Ferrés et al., 2013), with the exception of the study of small-scale PDCs presented by Bevilacqua et al. (2021). However, because the purpose of this latter application was illustrating the critical effect of using thematic vent opening maps, in it the authors deterministically imposed the PDCs formation conditions, and only varied vent position, paying limited attention to the expected characteristics of these PDCs.

Here we present a new probabilistic multi-hazard assessment for explosive volcanism at SSVC considering eruption scenarios characterized by both a central source and a significant uncertainty in vent position. We consider (a) large-scale pyroclastic fallout sourced from the central vent (Plinian and sub-Plinian volcanism), (b) small-volume pyroclastic fallout fed from Strombolian flank eruptions with uncertain position of the vent, (c) large-scale PDCs derived from the central vent (Plinian and sub-Plinian eruptions), and (d) small-scale PDCs generated during flank eruptions. We adopt a probabilistic approach to address the volcanic hazard, including wind seasonality in the study

of sub-Plinian eruptions, and we introduced novel, reproducible calibration procedures to set the inputs of our PDC numerical simulations (Aravena et al., 2022). Our results are limited to the assessment of volcanic hazard, thus considerations associated with the quantification of vulnerability and exposure are not included.

This paper is organized into five sections. In addition to the present introductory section, in Section 2 we present the main characteristics of SSVC. In Section 3, we describe the methods adopted to perform our numerical simulations and the definition of the input parameters. Results are presented in Section 4, including hazard maps for the different scenarios and eruption phenomena addressed here, followed by discussion and concluding remarks (Section 5).

2. Eruptive record of the SSVC and eruption scenarios

The Pleistocene-Holocene San Salvador Volcanic Complex (SSVC) is located in central El Salvador and is considered as one of the most hazardous volcanic complexes in Central America (Sofield, 2004; Ewert and Harpel, 2004; Figure 1). This volcanic field, part of the Central America Volcanic Arc, is made of El Boquerón stratovolcano, nested within the ancient volcanic edifice of San Salvador Volcano (SSV), and more than 25 monogenetic vents (Figure 1). The monogenetic vents include explosion craters, cinder cones and lava flows, being mainly arranged along two NW-trending normal fault systems.

The evolution of the SSVC can be divided into three phases (Sofield, 1998; Ferrés et al., 2011). The first phase (>70,000 – 36,000 yr BP) is associated with the construction of the old SSV and terminated with a large Plinian eruption that generated an elongated caldera, which has been described as sequence G-1. Cerro El Picacho and Cerro El Jabalí (Figure 1) are remnants of the deposits of this first stage of the evolution of the SSVC. Note that some new geochronology data of Ilopango Caldera eruptions (Cisneros de León et al., 2021) may modify the age limit between the first and the second evolution stage of the SSVC. During the second stage (36,000 – 3,000 yr BP), the active El Boquerón volcano was constructed inside this caldera, and volcanism was mainly concentrated at the central

vent. During the last 3,000 yr, which corresponds to the third stage of the evolution of the SSVC, volcanism was distributed on the flanks of the volcano and in the plain nearby, frequently involving phreatomagmatic activity. These monogenetic volcanic centers are equally distributed between scoria cones, in some cases associated with lava flows, and phreatomagmatic centers (explosion craters, tuff cones, tuff rings or maars; Ferrés et al., 2011). A recurrence period of ~133 yr for recent flank eruptions has been calculated by dividing the number of monogenetic centers by time (Ferrés et al., 2013). During this third stage (i.e., 3,000 yr – present), three explosive eruptions occurred at El Boquerón summit vent: Talpetate I (Toba de San Andrés; Hart, 1983), Talpetate II, and the most recent eruption in AD 1917. Talpetate I products were mainly distributed towards W-SW from the central vent (maximum dispersal of 18.9 km; Ferrés et al., 2011), while Talpetate II tephra dispersal occurred towards NNW. The sub-Plinian Talpetate I event is considered the most recent major explosive eruption in SSVC (column height of ~15 km). The 1917 eruption involved both effusive and explosive phases. It produced a'a lavas from a lateral fissure system on the northern flank of the main edifice and from inside the central crater, while a scoria cone (El Boqueroncito) grew inside the crater as a product of continuous Strombolian activity (column height of ~2 km).

Based on the eruptive record of SSVC, Sofield (2004) proposed five eruption scenarios: (1) a monogenetic magmatic eruption at the volcano flanks (VEI 1-3), which may involve the construction of a cinder cone, tephra deposits and lava flows; (2) a phreatomagmatic flank eruption (VEI 1-3), which would produce base surges and fallout deposits; (3) a small eruption at El Boquerón (VEI 1-3), whose products would include tephra fallout, ballistic fragments and possibly pyroclastic surges; (4) a sub-Plinian eruption at El Boquerón (VEI 4-5), involving tephra fallout, pyroclastic flows and pyroclastic surges; and (5) a Plinian eruption at El Boquerón (VEI 5-6), which would produce a widespread fallout deposit and pyroclastic flows. Ferrés et al. (2013) studied the scenarios associated with the central vent and presented specific deterministic hazard maps based on numerical

simulations. Here we extend this work by accounting for the uncertainty in eruption intensity and atmospheric conditions. In particular, we re-defined three eruption scenarios:

a. **ES1:** Plinian eruption at El Boquerón volcano.
b. **ES2:** Sub-Plinian event at El Boquerón volcano.
c. **ES3:** Small-scale (violent Strombolian) flank eruption.

3. Methods

3.1 Tephra fallout

3.1.1 Large-scale tephra fallout (ES1 and ES2)

We used the code TephraProb (Biass et al., 2016) to model the transport and deposition of tephra. This toolbox describes tephra dispersion using the advection-diffusion model Tephra2 (Bonadonna et al., 2005; 2012; Connor and Connor, 2006), and allows development of scenario-based probabilistic hazard assessments. The analytically solved advection-diffusion equation accounts for the influence in tephra dispersal of grain size distribution of pyroclasts, atmospheric conditions (i.e., wind field, which is assumed steady-state, vertically stratified but horizontally homogeneous) and eruption source parameters (such as plume height).,

We performed numerical simulations of two different eruption scenarios: Plinian eruption from the central vent and sub-Plinian eruption from the central vent (ES1 and ES2, respectively; Table 1). For sub-Plinian eruptions, we considered separately three periods: rainy season, dry season and the whole year. This is due to the marked shift in the wind patterns at middle altitudes (from 10 km a.s.l. to 20 km a.s.l.) between these two seasons (Figure 2) and the well-known effect of atmospheric conditions in tephra dispersal. The rainy season corresponds to the period between July and October (dominant wind direction at middle altitude towards WSW), while the dry season is the period from November to June (dominant wind direction at middle altitude towards ENE). The selected periods present the maximum differences in the wind field between the two seasons, although they are not strictly based on rainfall data. For Plinian eruptions we did not consider seasonality because minor differences are

observed in the wind field between 20 and 30 km a.s.l, which is the altitude range for the eruptive columns considered in this scenario and thus it is the zone where most of the mass is expected to be transported laterally. Atmospheric conditions were sampled from the NOAA NCEP/NCAR Reanalysis database (Kalnay et al., 1996), considering data from 1990 to 2020 by using ad-hoc procedures included in TephraProb. This database includes four daily values of wind speed and direction at 17 geopotential heights.

Following the sampling scheme described by Biass et al. (2016), for each eruption scenario, plume heights were stochastically sampled from a logarithmic distribution (i.e., uniform in logarithmic scale) to assign a higher weight to small events within the input range. Mass eruption rates can be computed from these height values. For each eruption scenario, eruption durations were sampled using a uniform distribution. However, when the sampled couple of column height and eruption duration gave rise to a total erupted mass outside the prescribed range for this parameter, this couple was discarded. Consequently, in practice, sampled eruption durations do not follow a uniform distribution. On the other hand, grain-size distribution parameters were sampled uniformly with no dependence on other model inputs. Numerical results are presented in terms of isolines of mass per unit area for different probability thresholds. Results indicate the expected range of mass load in the different zones of the volcano surroundings. Similarly, it is possible to produce hazard maps that, given a threshold of mass load on the ground, provide the probabilities of exceeding that value. All these probability values are conditioned on the occurrence of the selected eruption scenario (in this case, a sub-Plinian or Plinian eruption from the central vent of the SSVC).

3.1.2 Small-scale tephra fallout (ES3)

We also used the program TephraProb (Biass et al., 2016) to carry out one set of simulations for small-scale explosive eruptions (ES3, violent Strombolian volcanism; Table 1). Seasonality was not considered because variations in wind properties are only minor for heights lower than 8 km a.s.l. and thus they do not significantly affect the transport of pyroclasts in small-scale events as those modeled

here (Figure 2). Plume heights were uniformly sampled in logarithmic scale while eruption durations were sampled using a uniform distribution. We defined a range for erupted mass that limits the acceptable couples of plume height and eruption duration. Thus, in practice, eruption duration and column height were not sampled independently. To include the uncertainty in vent opening associated with these phenomena at the SSVC (Bevilacqua et al., 2021), we used a single vent position located at El Playón in the TephraProb simulations (Figure 1) and then we weighted our results inside the SSVC by adopting the averaged thematic map of vent opening for low-scale pyroclastic fallout presented by Bevilacqua et al. (2021), which is displayed in Figure S1a in the Supplementary material. The validity of this procedure lies on the small topography effect in the dispersion of tephra during explosive eruptions and the absence of systematic position-controlled variations in the wind field at the scale of the studied volcanic complex. Results are described in terms of isolines of exceedance probability for a set of thresholds of mass per unit area on the ground. These probabilities are conditioned on the occurrence of a violent Strombolian eruption at the SSVC with no assumptions associated with vent position.

3.2 Pyroclastic density currents

3.2.1 Large-scale pyroclastic density currents (ES1 and ES2)

To address pyroclastic density currents, we adopted the branching box model and the branching energy cone model (Aravena et al., 2020), as implemented in the programs BoxMapProb 2.0 and ECMapProb 2.0 (Aravena et al., 2022). They are modified formulations of the box model (Huppert and Simpson, 1980; Bonnecaze et al., 1995; Hallworth et al., 1998; Esposti Ongaro et al., 2016; Tadini et al., 2021b; Bevilacqua et al., 2022b) and the energy cone model (Malin and Sheridan, 1982; Sheridan and Malin, 1983; Wadge and Isaacs, 1988), respectively, and allow description of flow channelization with a limited computational cost (Aravena et al., 2020; Aravena and Roche, 2022). The applicability of these models depends on the nature of the PDCs described (Aravena et al., 2020). For the Plinian scenario (i.e. ES1), we used the branching box model because PDCs derived from

large-scale column collapse are expected to be dominantly inertial, while we considered both models to describe PDCs derived from partial column collapse during sub-Plinian events (i.e. ES2) because they may represent transitional currents between inertial and frictional flows. This choice was adopted to produce conservative results, even though field evidence suggests that the PDCs of the reference scenario (i.e., Talpetate I) were dominantly dilute.

We followed the procedures presented by Aravena et al. (2022) to calibrate the input variables. These structured, reproducible strategies are based on the geological record of the studied volcano and allow us to reduce the effect derived from arbitrary choices in the definition of simulation conditions (Aravena et al., 2022). We adopted the PDC deposits of eruptions G-1 and Talpetate I as reference inundation areas (Sofield, 1998; 2004; Ferrés et al., 2011; 2013) for ES1 and ES2, respectively. Note that the use of G-1 as a reference deposit may be considered questionable because these PDCs were emplaced in a different topographical context of the central edifice. However, as we show below, the effect of proximal topographic obstacles is of secondary importance in the resulting hazard maps associated with this scenario, with most of the simulations reaching and propagating over the plain nearby.

To construct calibrated PDC hazard maps, we performed different sets of calibration simulations using variable flow input parameters and fixed collapse positions at the summit of El Boquerón (Table 2). We compared the reference inundation area with the inundation areas computed in each calibration simulation using three different comparison metrics: Jaccard Index (JI), Hausdorff distance (HD) and root mean square distance (RMSD), which are defined as follows:

$$JI := \frac{|A \cap B|}{|A \cup B|} \tag{1}$$

$$HD := \max\left\{ \underset{i \in [1, n_r]}{\max} \left(\underset{j \in [1, n_r]}{\min} d(A_i, B_j) \right), \underset{i \in [1, n_r]}{\max} \left(\underset{j \in [1, n_r]}{\min} d(B_i, A_j) \right) \right\} \tag{2}$$

$$RMSD := \frac{\sqrt{\left(\sum_{i=1}^{n_r}\left(\min_{j \in [1,n_r]}\left(d(A_i,B_j)\right)^2\right)\right)+\left(\sum_{i=1}^{n_r}\left(\min_{j \in [1,n_r]}\left(d(B_i,A_j)\right)^2\right)\right)}}{2n_r} \quad (3)$$

where A is the reference inundation polygon, B is the inundation polygon associated with the calibration simulation under consideration, $d(\cdot,\cdot)$ is the function distance, and the subscripts refer to a series of $n_r = 1{,}000$ equidistant points along the borders of the two inundation polygons (i.e., reference inundation polygon and the one associated with the calibration simulation under consideration).

The above-mentioned metrics measure the level of overlap between the calibration simulations and the reference events, permitting us to define probability functions to sample calibrated sets of input parameters (Aravena et al., 2022). By means of this procedure, from each set of calibration simulations (Table 2), we sampled three sets of input parameters that derive from the independent application of the three comparison metrics mentioned above. On the other hand, collapse positions were sampled within the crater area and its rim (Table 2).

We used these inputs to perform a second group of simulations to construct calibrated hazard maps of PDC inundation (1,000 simulations for each one), which were combined to propose conservative hazard maps. In each inundation map, the results are described in terms of invasion probability, computed as the number of simulations that reach each pixel of the map over the total number of simulations. These probability values are conditioned on the occurrence of the specific eruption scenarios studied.

3.4 Small-scale pyroclastic density currents (ES3)

To address small-scale pyroclastic density currents related to violent Strombolian activity (i.e. ES3), we adopted exclusively the branching energy cone model (Aravena et al., 2020). This is because these phenomena are likely dominated by friction. Note that, even though some of the small-scale PDCs documented at the SSVC are associated with phreatomagmatic volcanism (maars and explosion craters), none of the SSVC monogenetic vents recognized during the last 1.6 ka (that is, after the

Tierra Blanca Joven eruption of Ilopango caldera; Pedrazzi et al., 2019) has presented a phreatomagmatic component (Ferrés et al., 2011; Ferrés et al., 2013; Bevilacqua et al., 2021), for which we have assumed that a frictional behaviour better represents the dynamics of future small-scale PDCs at the SSVC.

To extend the analysis presented in Bevilacqua et al. (2021), instead of the deterministic imposition of input parameters, we followed one of the calibration procedures presented by Aravena et al. (2022) and implemented it in ECMapProb 2.0. In particular, we performed a set of calibration simulations with input parameters variable within specific ranges (Table 2), using a fixed vent position at El Playón. From these simulations, ECMapProb 2.0 computes the runout distance associated with each pair of input parameters (Figure S2). Because of the lack of a detailed dataset of runout distance of past small-scale PDCs at the SSVC, and considering the typical values described in the literature, we assumed that a uniform distribution between 1 and 3 km is able to describe the range of runout distance associated with these phenomena at SSVC.

Using the information of the calibration simulations, input parameters were sampled in order to reproduce the prescribed distribution of runout distance. To sample the collapse position, we adopted the averaged thematic vent opening map presented by Bevilacqua et al. (2021) and displayed in Figure S1b. By coupling both sources of information, we performed a set of 10,000 numerical simulations considering variable PDC formation conditions that allows us to construct a calibrated PDC hazard map for ES3. In this case, results are described in terms of invasion probability, which is conditioned on the occurrence of a small-scale PDC at the SSVC, with no assumptions associated with the position of the vent.

4. Results

4.1 Tephra fallout

Figure 3 presents the hazard maps associated with the scenario of a Plinian eruption from El Boquerón volcano (ES1) crater, where we show different isolines of mass per unit area on the ground for three

probability thresholds: 10%, 50% and 90%. As expected, tephra dispersal occurs preferentially towards W-WSW, producing particularly high mass loads in Lourdes (of the order of 1000 kg/m^2 in the map of 50% of conditional probability; Figure 3). Results also indicate that a Plinian eruption similar to G-1 would likely produce ground mass loads between 100 and 1000 kg/m^2 in the metropolitan area of San Salvador city (50% of conditional probability), and also in other cities such as Santa Lucía, Quezaltepeque and Apopa. At distal zones, some of the cities that may be involved by significant tephra fallout during G-1-like Plinian eruptions are Coatepeque, Zaragoza, Jicalapa and Sonsonate, more than 40 km SW of El Boquerón volcano (ground mass loads of the order of 5-10 kg/m^2 in the map of 50% of conditional probability). In these simulations, the expected areas with mass loads higher than 1000 kg/m^2, 100 kg/m^2 and 10 kg/m^2 are 124 km^2, 453 km^2 and 1609 km^2, respectively.

Results for sub-Plinian tephra fallout sourced from the central vent (ES2) are shown in Figure 4. Results assuming the wind distribution for the whole year are displayed in Figure S3 in the Supplementary Material. Seasonal winds strongly control the expected dispersal of tephra during sub-Plinian eruptions at El Boquerón volcano (Ferrés et al., 2013), with a large increase of the probability of tephra dispersal toward the eastern quadrants for eruptions occurring during the dry season (Figure 4). For instance, in the San Salvador metropolitan area, the expected ground mass load is of the order of 1-10 kg/m^2 (50% of conditional probability) but unfavorable wind conditions, which are significantly more likely during the dry season, may result in mass loads of the order of 100 kg/m^2 (Figure 4). The expected mass load at Lourdes is of ~100 kg/m^2 (50% of conditional probability), while distal cities that may be involved by significant tephra fallout during sub-Plinian eruptions at El Boquerón volcano are Sacacoyo and Santa Lucía, in the radius of 20 km from El Boquerón volcano. In this eruption scenario, the expected areas with mass loads higher than 1000 kg/m^2, 100 kg/m^2 and 10 kg/m^2 are 24 km^2, 95 km^2 and 344 km^2, respectively. These results, especially those associated with the rainy season, are consistent with the dispersal axis observed for Talpetate I

eruption (Sofield, 2004), which presents tephra loads of the order of those observed in the isopach map of 50% of conditional probability (Figure 4).

Tephra fallout produced during violent Strombolian eruptions from monogenetic centers (ES3) have maximum probabilities of significant tephra sedimentation are computed in the NW flank of San Salvador volcano, in the surroundings of the village of Nuevo Sitio del Niño (Figure 5). The maximum conditional probability of depositing a mass load higher than 10 kg/m^2 is slightly higher than 7%, while the maximum conditional probability is lower than 4% when a ground mass load of 100 kg/m^2 is considered. Our results show very low conditional probabilities for the metropolitan area of San Salvador and Lourdes for any relevant threshold of tephra mass load during violent Strombolian events (ES3).

4.2 Pyroclastic density currents

The PDC hazard maps associated with column collapse during Plinian (ES1) and sub-Plinian (ES2) eruptions at the central vent of SSVC are presented in Figure 6 and 7. In order to present conservative results, these figures were constructed considering, for each pixel, the maximum inundation probability calculated in a set of hazard maps computed through different models (branching box model for ES1 and ES2 and branching energy cone model for ES2) and, in the case of the branching box model, different values of sedimentation velocity (see Table 2 and Supplementary Figures S4-S7). The sedimentation velocity is a poorly constrained parameter which can significantly affect the branching box model results (Bevilacqua et al., 2022b), but it is kept fixed in the calibration procedures presented by Aravena et al. (2022). Thus, by considering calibrations with different sedimentation velocities, in this work we explore the uncertainty associated with the three input parameters that mostly control the results of the branching box model (i.e., collapsing volume, initial concentration of pyroclasts, and sedimentation velocity; Table 2). Note that the adopted sedimentation velocities are related to grain sizes of the order of tens to a few hundreds of microns (Le Roux, 1992; Dellino et al., 2019).

Pyroclastic density currents produced during Plinian eruptions are able to inundate a significant portion of the volcano flanks and the nearby plain, involving partially or completely cities such as San Salvador (30-70% of conditional probability, Figures 6 and S4-5), Santa Tecla (40-70%), Quezaltepeque (~30%), Nuevo Sitio del Niño (~30%), Lourdes (~30-40%), and Apopa (~10-20%). Cerro El Picacho has a clear effect reducing the PDC hazard in the metropolitan area of San Salvador (Figs. 6 and S4), even though the resulting conditional inundation probability in San Salvador is still significant, with most simulations overcoming the proximal topographic obstacles. In our simulations, the mean value of runout distance ranges between 7.4 km (RMSD calibration and sedimentation velocity of 0.30 m/s or 1.20 m/s) and 14.3 km (JI calibration and sedimentation velocity of 0.05 m/s), while the mean value of the inundation area varies between 178.4 km^2 (RMSD calibration and sedimentation velocity of 1.20 m/s) and 438.9 km^2 (JI calibration and sedimentation velocity of 0.05 m/s). The inundation area associated with large-scale PDCs is strongly consistent with the reference scenario used for model calibration, with most of the distal outcrops of G-1 (Ferrés et al., 2013) being contained between the contour lines of 5% and 20% of inundation probability (Figure 6).

PDCs derived from partial eruption column collapse during sub-Plinian events show propagation dynamics strongly controlled by the proximal topography of the volcano, especially Cerro El Picacho (Figures 7 and S6-8). Most of the simulations only reach the flanks of the volcano, and only a minor portion of our simulations is able to propagate onto peripheral zones of San Salvador and Santa Tecla, with conditional probabilities lower than 5%. For simulations performed using the branching box model, the mean value of runout distance ranges between 1.5 (RMSD calibration and sedimentation velocity of 1.20 m/s) and 2.1 km (JI calibration and sedimentation velocity of 0.05 m/s), and the mean value of inundation area varies between 9.0 km^2 (RMSD calibration and sedimentation velocity of 1.20 m/s) and 13.2 km^2 (HD calibration and sedimentation velocity of 0.05 m/s). On the other hand, for the branching energy cone model simulations, the mean value of runout distance varies between

2.9 km (RMSD calibration) and 3.2 km (JI calibration) and the mean inundation area ranges from 11.1 km^2 (RMSD calibration) to 16.0 km^2 (HD calibration). Note that both sets of results are expected to be different because the models describe different types of PDCs. The results presented in Figure 7 integrate both sources of information using a conservative approach. The inundation area of the reference pyroclastic flow, which is reported in Sofield (2004), is contained within the contour line of ~10% of inundation probability (Figure 7).

Figure 8 illustrates the inundation map of small-scale PDCs derived from violent Strombolian volcanism (ES3), considering a source distributed along a large part of the volcanic field (Bevilacqua et al., 2021). Maximum inundation probabilities are computed in the NW flank of the volcano, with values slightly higher than 10%; significant invasion probabilities are observed in Nuevo Sitio del Niño (~5%). The inundation probability in the metropolitan area of San Salvador is very low (<1%). Our inundation probabilities are lower compared to the hazard maps presented by Bevilacqua et al. (2021). Differences derive from the application in this study of a structured calibration procedure. Bevilacqua et al. (2021) imposed deterministically the input parameters of the branching energy cone model, and thus, as the authors mentioned, their results are valid only for specific conditions of PDC size and friction parameter. On the other hand, here we sampled the input parameters in order to reproduce a prescribed distribution of runout distance. We highlight that calibration simulations were performed only at a specific location, while the final simulations were developed in different zones of the studied volcanic field. This may produce differences between the prescribed distribution of runout distance and the final simulations, although the low-relief topography should strongly reduce this effect. In this case, the main value of runout in the resulting distribution of runout distance is about 2.1 km, slightly higher than the mean value of the prescribed distribution. On the other hand, the mean value of the simulated inundation area is 11.6 km^2 with a median value of 7.8 km^2.

5. Discussion and conclusion

The adoption of an appropriate approach to address volcanic hazard at a given volcanic system depends on its specificities (Calder et al., 2015). For instance, although vent position does not typically need to be treated as a variable parameter in central volcanoes, this parameter is one of the main factors controlling hazard and risk in systems dominated by monogenetic volcanism or characterized by both central vents and flank eruptions (e.g., Barsotti et al., 2010; Del Negro et al., 2013; Neri et al., 2015; Ang et al., 2020; Bevilacqua et al., 2021; Sieron et al., 2014; 2021). This is the case of the San Salvador Volcanic Complex, El Salvador. In this work, we have assessed different volcanic hazards associated with this volcanic system, considering a set of likely eruption scenarios initially proposed by Sofield (2004) and lately discussed by Ferrés et al. (2013). This work, building on numerous previous studies including those just mentioned (Sofield, 1998, 2004; Major et al., 2011; Ferrés et al., 2011, 2013; Bevilacqua et al., 2021), represents a further step forward in our understanding of this volcanic field due to the following two reasons:

(a) In contrast to previous hazard assessment studies, we include here the analysis of monogenetic volcanism by coupling vent opening probability maps (Bevilacqua et al., 2021) with tephra fallout and PDC numerical models (Biass et al., 2016; Aravena et al., 2020). This is particularly relevant for the SSVC because a monogenetic eruption is the most probable future event in this volcanic system, with a recurrence period of about 133 yr based on data from the last 1,000 years (Ferrés et al., 2013). It is worth noting that our study also considers the occurrence of eruptions sourced from main central vent.

(b) Differently from previous hazard studies, we adopted a fully probabilistic approach to analyze the different eruption scenarios considered here, based on the development of large sets of numerical simulations with variable input parameters for the two eruption phenomena here studied. Moreover, the model input parameters were imposed by using reproducible calibration and sampling strategies (Biass et al., 2016; Aravena et al., 2022) able to generate robust numerical results.

In this way, our strategy deals simultaneously with the uncertainty in vent position, magnitude and intensity of future eruptions; the possible correlation between vent position and eruption style; and the dispersal dynamics of volcanic products in the atmosphere and along the volcano flanks.

The integration of results derived from the analysis of different eruption scenarios of central volcanism and flank eruptions in a single hazard map is a challenging task that allows simplifying the information that must be communicated to decision makers and the population, for which the development of event trees has been a commonly applied strategy (e.g., Sobradelo and Marti, 2010; Sieron et al., 2019; Ang et al., 2020). However, key information for hazard assessment may be missed during this process, particularly in presence of significant uncertainty in the recurrence time associated with different eruption scenarios. In this study case, while a ~133 yr recurrence period was computed for recent flank eruptions (Ferrés et al., 2013), the recurrence period for sub-Plinian explosive events at El Boquerón volcano is poorly constrained, even though we can suggest it is one order of magnitude larger than that of flank events; while the uncertainty associated with Plinian eruptions is even higher. For this reason, in this work we have decided not to integrate the hazard maps associated with the different eruptive scenarios.

Tephra fallout

Results indicate that a Plinian eruption at El Boquerón volcano (plume height of 20 – 30 km) could produce significant tephra sedimentation in the metropolitan area of San Salvador, with the potential of reaching ground mass loads of the order of 100 kg/m^2 under unfavorable wind conditions. Other cities that may be affected by this type of activity are Lourdes, Santa Lucía, Zaragoza, Sonsonate, Quezaltepeque, Apopa, and, less probably, Coatepeque, Jujutla and Acajutla. It is also relevant to note that this scenario may affect dramatically the road infrastructure to the west of El Salvador (e.g., the Pan-American Highway).

The potential effect of sub-Plinian eruptions (plume height of 12 – 20 km) is significantly smaller and strongly influenced by the seasonality of wind. For instance, 50% of our simulations during the

dry season produce tephra mass loads of the order of 10 kg/m^2 in the metropolitan area of San Salvador, while tephra mass loads of the order of only 1 kg/m^2 are likely during the rainy season.

Finally, the potential of flank eruptions to produce significant tephra deposition in the metropolitan area is small compared to those of the previously discussed scenarios. The maximum probabilities of producing thick fallout deposits derived from flank eruptions are near the NW flank of the volcano (~7% for a tephra mass load of 10 kg/m^2; ~3% for a tephra mass load of 100 kg/m^2), which is a consequence of the characteristics of the thematic vent opening map of small-scale pyroclastic fallout of SSVC (Figure S1; Bevilacqua et al., 2021). Other cities that may be affected by this type of activity are Lourdes, Santa Lucía and Sacacoyo.

Pyroclastic density currents

PDCs as those derived from the column collapse of catastrophic Plinian events have the potential of invading a significant portion of the volcano surroundings and part of the metropolitan area of San Salvador and Santa Tecla, while significant inundation probabilities are also computed for Lourdes, Quezaltepeque and Nuevo Sitio del Niño (15-40% of conditional probability). In this case, the effect of the topographic barriers such as Cerro el Picacho and Cerro El Jabali is insufficient to protect the most populated cities in the volcano surroundings. Note, however, that this eruption scenario has been extremely infrequent in the eruption record of SSVC and its occurrence probability is thus expected to be small.

PDCs derived from partial column collapse during sub-Plinian events (reference event such as Talpetate I) show a strong control of the volcano topography, with a significant barrier effect exerted by Cerro El Picacho. Low invasion probabilities were computed for San Salvador (of the order of 1% of conditional probability), Lourdes (<1%) and Quezaltepeque (<1%), even though the rapid expansion of the metropolitan area of San Salvador and Santa Tecla towards the flank of the central volcano may result in significant invasion probabilities (up to 5% of probability) in the proximal urbanized areas.

Finally, small-scale PDCs derived from small-scale magmatic volcanism (Bevilacqua et al., 2021) present their maximum inundation probabilities at the NW flank of the volcano, with a peak of about 10%, and low inundation probabilities in the metropolitan area of San Salvador city.

Comparison with results of Ferrés et al. (2013)

Because our analysis presents significant differences with the study presented by Ferrés et al. (2013), direct results comparison is not straightforward. However, we can mention some key points:

(a) Although the names used to define each eruption scenario differ from those of Ferrés et al (2013), the variation ranges adopted for column height in the scenarios ES1 and ES2 are consistent between the two studies. Moreover, the geometry of the isomass maps associated with a conditional probability of 50% (i.e. Figures 4 and S3) are remarkably consistent with the isopach maps presented by Ferrés et al. (2013). On the other hand, we do not include comparisons for ES3 because Ferrés et al. (2013) did not model flank volcanism.

(b) Regarding PDCs, Ferrés et al. (2013) separately considered pyroclastic flows and pyroclastic surges, and defined scenarios for them based on different documented events, which hinders the identification of equivalences between our maps and those of Ferrés et al. (2013). However, both studies recognize the relevant effect of Cerro El Picacho and Cerro El Jabali in the propagation dynamics of small-scale PDCs and their observable but limited influence for large-scale PDCs. The most energetic scenario defined by Ferrés et al. (2013) for PDCs is reasonably consistent with the 20% isoline presented in Figure 6, even though our simulations show higher inundation probabilities across the Cordillera del Bálsamo (south of San Salvador). Finally, both studies suggest a relevant effect of distal topographic obstacles north of Quezaltepeque city in limiting the propagation of large-scale PDCs in the SSVC.

Limitations of the study and open questions

The main limitation of this scenario-based probabilistic hazard assessment is that it is conditional on the occurrence of a given eruptive scenario and therefore does not provide information on the

recurrence period of the eruption scenarios addressed, making it difficult to calculate the associated long-term occurrence probabilities (Sobradelo and Martí, 2010; Garcia-Aristizabal et al., 2013; Connor et al., 2015; Bevilacqua et al., 2017a; 2020; 2022c). Probabilistic hazard maps conditioned to the occurrence of a given event are, however, the more common result in modern volcanic hazard studies, and do not include the generally high uncertainty associated with the estimation of the occurrence probability of a given eruption. In addition, these kinds of maps have larger applicability, as they can be combined *a posteriori* with the value of probability of occurrence of a given event.

An additional limitation of our study relates to the subjective definition of likely eruption scenarios and reference events to characterize them, which also hinders the development of a full comparison between our hazard maps and those present in the literature. In the case of tephra fallout, we accounted for the expected variation range of column height during explosive eruptions, whereas the definition of inputs for PDC simulations based on the calibration strategies proposed by Aravena et al. (2022) translates into a discrete set of scenarios which may not cover all the different scales of PDCs observed in nature. Numerical modeling of PDCs of intermediate volume between ES1 and ES2 could help to better understand the propagation dynamics of PDCs in SSVC, but the absence of field data potentially useful to calibrate numerical models hinders the analysis of this eruption scenario. For the eruption scenarios considered in this work, the choice of the models adopted to describe PDCs is based on the magnitude of the eruptions, assuming that small-scale PDCs are frictional and large-scale PDCs are mainly dominated by inertia. This simplistic assumption may represent an additional limitation of our approach.

This contribution complements a significant number of studies on SSVC (Fairbrother et al., 1978; Sofield, 1998; 2004; Major et al., 2001; Ferrés et al., 2011; 2013) by presenting new probabilistic hazard maps for different scenarios of central and distributed explosive volcanism. However, we believe that both the eruption record of SSVC and the presence of highly populated cities in the surrounding areas, support the need to further develop these studies with the aim of improving our

understanding of the behavior of this volcanic system and the quantification of the associated hazards. We also suggest that useful future investigations would be, for instance, the analysis and numerical modeling of lava flows and studies related to the quantification of exposure and vulnerability of the surrounding communities, in order to produce a comprehensive dataset and therefore provide a first estimate of volcanic risk in the San Salvador metropolitan area.

Acknowledgements

This research was supported by the RIESCA project, funded by the Italian Agency for Development Cooperation and aimed at promoting applied training in risk scenarios in Central America. AA was financed by the French government IDEX-ISITE initiative 16-IDEX-0001 (CAP 20-25). The constant coordination and support to the project by Giuseppe Giunta is greatly acknowledged.

References

Ang, P.S., Bebbington, M.S., Lindsay, J.M., Jenkins, S.F., 2020. From eruption scenarios to probabilistic volcanic hazard analysis: An example of the Auckland Volcanic Field, New Zealand. Journal of Volcanology and Geothermal Research, 397, 106871. https://doi.org/10.1016/j.jvolgeores.2020.106871

Aravena, A., Cioni, R., Bevilacqua, A., de' Michieli Vitturi, M., Esposti Ongaro, T., Neri, A., 2020. Tree- branching- based enhancement of kinetic energy models for reproducing channelization processes of pyroclastic density currents. Journal of Geophysical Research: Solid Earth, 125(7), e2019JB019271. https://doi.org/10.1029/2019JB019271

Aravena, A., Cioni, R., Bevilacqua, A., de' Michieli Vitturi, M., Esposti Ongaro, T., Neri, A., 2022. Calibration strategies of PDC kinetic energy models and their application to the construction of hazard maps. Bulletin of Volcanology, 84(3), 1-21. https://doi.org/10.1007/s00445-022-01538-8

Aravena, A., Roche, O., 2022. Influence of the topography of stratovolcanoes on the propagation and channelization of dense pyroclastic density currents analyzed through numerical simulations. Bulletin of Volcanology, 84(7), 1-12. https://doi.org/10.1007/s00445-022-01576-2

Barsotti, S., Andronico, D., Neri, A., Del Carlo, P., Baxter, P.J., Aspinall, W.P., Hincks, T., 2010. Quantitative assessment of volcanic ash hazards for health and infrastructure at Mt. Etna (Italy) by numerical simulation. Journal of Volcanology and Geothermal Research, 192(1-2), 85-96. https://doi.org/10.1016/j.jvolgeores.2010.02.011

Becerril, L., Bartolini, S., Sobradelo, R., Martí, J., Morales, J.M., Galindo, I., 2014. Long-term volcanic hazard assessment on El Hierro (Canary Islands). Natural Hazards and Earth System Sciences, 14(7), 1853-1870. https://doi.org/10.5194/nhess-14-1853-2014

Bevilacqua, A., Isaia, R., Neri, A., Vitale, S., Aspinall, W.P., Bisson, M., Flandoli, F., Baxter, P.J., Bertagnini, A., Esposti Ongaro, T., Iannuzzi, E., Pistolesi, M., Rosi, M., 2015. Quantifying volcanic hazard at Campi Flegrei caldera (Italy) with uncertainty assessment: 1. Vent opening maps. Journal of Geophysical Research: Solid Earth, 120(4), 2309-2329. https://doi.org/10.1002/2014JB011775

Bevilacqua, A., Flandoli, F., Neri, A., Isaia, R., Vitale, S., 2016. Temporal models for the episodic volcanism of Campi Flegrei caldera (Italy) with uncertainty quantification. Journal of Geophysical Research: Solid Earth, 121(11), 7821-7845. https://doi.org/10.1002/2016JB013171

Bevilacqua, A., Neri, A., Bisson, M., Esposti Ongaro, T., Flandoli, F., Isaia, R., Rosi, M., Vitale, S., 2017a. The effects of vent location, event scale, and time forecasts on pyroclastic density current hazard maps at Campi Flegrei caldera (Italy). Frontiers in Earth Science, 5, 72. https://doi.org/10.3389/feart.2017.00072

Bevilacqua, A., Bursik, M., Patra, A., Pitman, E.B., Till, R., 2017b. Bayesian construction of a long-term vent opening probability map in the Long Valley volcanic region (CA, USA). Statistics in Volcanology, 3(1), 1. http://dx.doi.org/10.5038/2163-338X.3.1

Bevilacqua, A., Bursik, M., Patra, A., Pitman, E.B., Yang, Q., Sangani, R., Kobs- Nawotniak, S., 2018. Late Quaternary eruption record and probability of future volcanic eruptions in the Long Valley volcanic region (CA, USA). Journal of Geophysical Research: Solid Earth, 123(7), 5466-5494. https://doi.org/10.1029/2018JB015644

Bevilacqua, A., Bertagnini, A., Pompilio, M., Landi, P., Del Carlo, P., Di Roberto, A., Aspinall, W., Neri, A., 2020. Major explosions and paroxysms at Stromboli (Italy): A new historical catalog and temporal models of occurrence with uncertainty quantification. Scientific Reports, 10(1), 1-18. https://doi.org/10.1038/s41598-020-74301-8

Bevilacqua, A., Aravena, A., Neri, A., Gutiérrez, E., Escobar, D., Schliz, M., Aiuppa, A., Cioni, R., 2021. Thematic vent opening probability maps and hazard assessment of small-scale pyroclastic density currents in the San Salvador volcanic complex (El Salvador) and Nejapa-Chiltepe volcanic complex (Nicaragua). Natural Hazards and Earth System Sciences, 21, 1639-1665. https://doi.org/10.5194/nhess-21-1639-2021

Bevilacqua, A., Macedonio, G., Neri, A., Orsi, G., Petrosino, P., 2022a. Volcanic Hazard Assessment at the Campi Flegrei Caldera, Italy. In: Campi Flegrei (pp. 311-355). Springer, Berlin, Heidelberg. https://doi.org/10.1007/978-3-642-37060-1_12

Bevilacqua, A., Aravena, A., Aspinall, W., Costa, A., Mahony, S., Neri, A., Sparks, S., Hill, B., 2022b. Assessing minimum pyroclastic density current mass to impact critical infrastructures: example from Aso Caldera (Japan). Natural Hazards and Earth System Sciences , 22(10), 3329-3348. https://doi.org/10.5194/nhess-22-3329-2022

Bevilacqua, A., Azzaro, R., Branca, S., D'Amico, S., Flandoli, F., Neri, A., 2022c. Quantifying the statistical relationships between flank eruptions and major earthquakes at Mt. Etna volcano (Italy). Journal of Geophysical Research: Solid Earth, e2022JB024145. https://doi.org/10.1029/2022JB024145

Biass, S., Bonadonna, C., Connor, L., Connor, C., 2016. TephraProb: a Matlab package for probabilistic hazard assessments of tephra fallout. Journal of Applied Volcanology, 5(1), 1-16. https://doi.org/10.1186/s13617-016-0050-5

Bonadonna, C., Connor, C.B., Houghton, B.F., Connor, L., Byrne, M., Laing, A., Hincks, T.K., 2005. Probabilistic modeling of tephra dispersal: Hazard assessment of a multiphase rhyolitic eruption at Tarawera, New Zealand. Journal of Geophysical Research: Solid Earth, 110(B3). https://doi.org/10.1029/2003JB002896

Bonadonna, C., Folch, A., Loughlin, S., Puempel, H., 2012. Future developments in modelling and monitoring of volcanic ash clouds: outcomes from the first IAVCEI-WMO workshop on Ash Dispersal Forecast and Civil Aviation. Bulletin of Volcanology, 74(1), 1-10. https://doi.org/10.1007/s00445-011-0508-6

Bonnecaze, R., Hallworth, M., Huppert, H., Lister, J., 1995. Axisymmetric particle-driven gravity currents. Journal of Fluid Mechanics, 294, 93– 121. https://doi.org/10.1017/S0022112095002825

Calder, E., Wagner, K., Ogburn, S., 2015. Volcanic hazard maps. Global volcanic hazards and risk, 335-342. https://doi.org/10.1017/CBO9781316276273.022

Cioni, R., Longo, A., Macedonio, G., Santacroce, R., Sbrana, A., Sulpizio, R., Andronico, D., 2003. Assessing pyroclastic fall hazard through field data and numerical simulations: example from Vesuvius. Journal of Geophysical Research: Solid Earth, 108(B2). https://doi.org/10.1029/2001JB000642

Cioni, R., Bertagnini, A., Santacroce, R., Andronico, D., 2008. Explosive activity and eruption scenarios at Somma-Vesuvius (Italy): towards a new classification scheme. Journal of Volcanology and Geothermal Research, 178(3), 331-346. https://doi.org/10.1016/j.jvolgeores.2008.04.024

Cisneros de León, A., Schmitt, A., Kutterolf, S., Schindlbeck- Belo, J., Hernández, W., Sims, K., Garrison, J., Kant, L., Weber, B. Wang, K., Trumbull, R., 2021. Zircon and melt extraction from a long- lived and vertically extensive magma system underneath Ilopango Caldera (El Salvador). Geochemistry, Geophysics, Geosystems, 22(5), e2020GC009507. https://doi.org/10.1029/2020GC009507

Connor, L.J., Connor, C.B., 2006. Inversion is the key to dispersion: understanding eruption dynamics by inverting tephra fallout. In: Statistics in Volcanology. The Geological Society, p. 231-242. https://doi.org/10.1144/IAVCEI001.18

Connor, C., Bebbington, M., Marzocchi, W., 2015. Probabilistic volcanic hazard assessment. In The Encyclopedia of Volcanoes (pp. 897-910). Academic Press. https://doi.org/10.1016/B978-0-12-385938-9.00051-1

Costa, A., Dell'Erba, F., Di Vito, M. A., Isaia, R., Macedonio, G., Orsi, G., Pfeiffer, T., 2009. Tephra fallout hazard assessment at the Campi Flegrei caldera (Italy). Bulletin of Volcanology, 71(3), 259-273. https://doi.org/10.1007/s00445-008-0220-3

Del Negro, C., Cappello, A., Neri, M., Bilotta, G., Hérault, A., Ganci, G., 2013. Lava flow hazards at Mount Etna: constraints imposed by eruptive history and numerical simulations. Scientific Reports, 3(1), 1-8. https://doi.org/10.1038/srep03493

Dellino, P., Dioguardi, F., Doronzo, D.M., Mele, D., 2019. The rate of sedimentation from turbulent suspension: An experimental model with application to pyroclastic density currents and discussion on the grain- size dependence of flow runout. Sedimentology, 66(1), 129-145. https://doi.org/10.1111/sed.12485

Doronzo, D.M., Di Vito, M.A., Arienzo, I., Bini, M., Calusi, B., Cerminara, M., Corradini, S., de Vita, S., Giaccio, B., Gurioli, L., Mannella, G., Ricciardi, G.P., Rucco, I., Sparice, D., Todesco, M., Trasatti, E., Zanchetta, G., 2022. The 79 CE eruption of Vesuvius: A lesson from the past and the need of a multidisciplinary approach for developments in volcanology. Earth-Science Reviews, 104072. https://doi.org/10.1016/j.earscirev.2022.104072

Esposti Ongaro, T., Neri, A., Todesco, M., Macedonio, G., 2002. Pyroclastic flow hazard assessment at Vesuvius (Italy) by using numerical modeling. II. Analysis of flow variables. Bulletin of Volcanology, 64(3-4), 178-191. https://doi.org/10.1007/s00445-001-0190-1

Esposti Ongaro, T., Neri, A., Menconi, G., de' Michieli Vitturi, M., Marianelli, P., Cavazzoni, C., Erbacci, G., Baxter, P.J., 2008. Transient 3D numerical simulations of column collapse and pyroclastic density current scenarios at Vesuvius. Journal of Volcanology and Geothermal Research, 178(3), 378-396. https://doi.org/10.1016/j.jvolgeores.2008.06.036

Esposti Ongaro, T., Orsucci, S., Cornolti, F., 2016. A fast, calibrated model for pyroclastic density currents kinematics and hazard. Journal of Volcanology and Geothermal Research, 327, 257–272. https://doi.org/10.1016/j.jvolgeores.2016.08.002

Ewert, J.W., Harpel, C.J., 2004. In harm's way: population and volcanic risk. Geotimes, 49(4), 14-17.

Fairbrothers, G.E., Carr, M.J., Mayfield, D.G., 1978. Temporal magmatic variation at Boquerón volcano, El Salvador. Contributions to Mineralogy and Petrology, 67(1), 1-9. https://doi.org/10.1007/BF00371627

Ferrés, D., Granados, H.D., Hernández, W., Pullinger, C., Chávez, H., Taracena, C.C., Cañas-Dinarte, C., 2011. Three thousand years of flank and central vent eruptions of the San Salvador volcanic complex (El Salvador) and their effects on El Cambio archeological site: a review based on tephrostratigraphy. Bulletin of Volcanology, 73(7), 833-850. https://doi.org/10.1007/s00445-011-0465-0

Ferrés, D., Granados, H.D., Gutiérrez, R.E., Farraz, I.A., Hernández, E.W., Pullinger, C.R., Escobar, C.D., 2013. Explosive volcanic history and hazard zonation maps of Boquerón Volcano (San Salvador volcanic complex, El Salvador). Geological Society of America Special Papers, 4(498), 201-230. https://doi.org/10.1130/2013.2498(12)

Garcia-Aristizabal, A., Selva, J., Fujita, E., 2013. Integration of stochastic models for long-term eruption forecasting into a Bayesian event tree scheme: a basis method to estimate the probability of volcanic unrest. Bulletin of Volcanology, 75(2), 1-13. https://doi.org/10.1007/s00445-013-0689-2

Gueugneau, V., Kelfoun, K., Charbonnier, S., Germa, A., Carazzo, G., 2020. Dynamics and impacts of the May 8th, 1902 pyroclastic current at Mount Pelée (Martinique): new insights from numerical modeling. Frontiers in Earth Science, 8, 279. https://doi.org/10.3389/feart.2020.00279

Kalnay, E., Kanamitsu, M., Kistler, R., Collins, W., Deaven, D., Gandin, L., Iredell, M., Saha, S., White, G., Woollen, J., Zhu, Y., Chelliah, M., Ebisuzaki, W., Higgins, W., Janowiak, J., Mo, K. C., Ropelewski, C., Wang, J., Leetmaa, A., Reynolds, R., Jenne, R., Joseph, D., 1996. The NCEP/NCAR 40-year reanalysis project. Bulletin of the American Meteorological Society, 77(3), 437-472. https://doi.org/10.1175/1520-0477(1996)077<0437:TNYRP>2.0.CO;2

Hallworth, M., Hogg, A., Huppert, H., 1998. Effects of external flow on compositional and particle gravity currents. Journal of Fluid Mechanics, 359, 109– 142. https://doi.org/10.1017/S0022112097008409

Hart, W., 1983. Classic to Postclassic Tephra exposed in Archeological sites, Eastern Zapotitán Valley of El Salvador. In: Sheets P (ed) Archeology and Volcanism in Central America University of Texas Press, Austin, 44-51. https://doi.org/10.7560/787087-004

Huppert, H., Simpson, J., 1980. The slumping of gravity currents. Journal of Fluid Mechanics, 99(4), 785– 799. https://doi.org/10.1017/S0022112080000894

Le Roux, J., 1992. Settling velocity of spheres: a new approach. Sedimentary Geology, 81(1-2), 11-16. https://doi.org/10.1016/0037-0738(92)90053-T

Macedonio, G., Costa, A., Folch, A., 2008. Ash fallout scenarios at Vesuvius: numerical simulations and implications for hazard assessment. Journal of Volcanology and Geothermal Research, 178(3), 366-377. https://doi.org/10.1016/j.jvolgeores.2008.08.014

Macedonio, G., Costa, A., Scollo, S., Neri, A., 2016. Effects of eruption source parameter variation and meteorological dataset on tephra fallout hazard assessment: example from Vesuvius (Italy). Journal of Applied Volcanology, 5(1), 1-19. https://doi.org/10.1186/s13617-016-0045-2

Major, J.J., Schilling, S.P., Sofield, D.J., Escobar, C.D., Pullinger, C.R., 2001. Volcano hazards in the San Salvador region, El Salvador. Open-file Report. U. S. Geological Survey, (366), 28.

Malin, M.C., Sheridan, M.F., 1982. Computer-assisted mapping of pyroclastic surges. Science, 217(4560), 637-640. https://doi.org/10.1126/science.217.4560.637

Martí, J., Sobradelo, R., Felpeto, A., García, O., 2012. Eruptive scenarios of phonolitic volcanism at Teide–Pico Viejo volcanic complex (Tenerife, Canary Islands). Bulletin of Volcanology, 74(3), 767-782. https://doi.org/10.1007/s00445-011-0569-6

Neri, A., Aspinall, W.P., Cioni, R., Bertagnini, A., Baxter, P.J., Zuccaro, G., Andronico, D., Barsotti, S., Cole, P.D., Esposti Ongaro, T., Hincks, T.K., Macedonio, G., Papale, P., Rosi, M., Santacroce, R., Woo, G., 2008. Developing an event tree for probabilistic hazard and risk assessment at Vesuvius. Journal of Volcanology and Geothermal Research, 178(3), 397-415. https://doi.org/10.1016/j.jvolgeores.2008.05.014

Neri, A., Bevilacqua, A., Esposti Ongaro, T., Isaia, R., Aspinall, W.P., Bisson, M., Flandoli, F., Baxter, P.J., Bertagnini, A., Iannuzzi, E., Orsucci, S., Pistolesi, M., Rosi, M., Vitale, S., 2015. Quantifying volcanic hazard at Campi Flegrei caldera (Italy) with uncertainty assessment: 2. Pyroclastic density current invasion maps. Journal of Geophysical Research: Solid Earth, 120(4), 2330-2349. https://doi.org/10.1002/2014JB011776

Orsi, G., Di Vito, M.A., Selva, J., Marzocchi, W., 2009. Long-term forecast of eruption style and size at Campi Flegrei caldera (Italy). Earth and Planetary Science Letters, 287(1-2), 265-276. https://doi.org/10.1016/j.epsl.2009.08.013

Pedrazzi, D., Sunye-Puchol, I., Aguirre-Díaz, G., Costa, A., Smith, V.C., Poret, M., Dávila-Harris, P., Miggins, D.P., Hernández, W., Gutiérrez, E., 2019. The Ilopango Tierra Blanca Joven (TBJ) eruption, El Salvador: volcano-stratigraphy and physical characterization of the major Holocene event of Central America. Journal of Volcanology and Geothermal Research, 377, 81-102. https://doi.org/10.1016/j.jvolgeores.2019.03.006

Pistolesi, M., Cioni, R., Rosi, M., Aguilera, E., 2014. Lahar hazard assessment in the southern drainage system of Cotopaxi volcano, Ecuador: Results from multiscale lahar simulations. Geomorphology, 207, 51-63. https://doi.org/10.1016/j.geomorph.2013.10.026

Rabus, B., Eineder, M., Roth, A., Bamler, R., 2003. The shuttle radar topography mission—A new class of digital elevation models acquired by spaceborne radar. ISPRS Journal of Photogrammetry and Remote Sensing, 57(4), 241– 262. https://doi.org/10.1016/S0924-2716(02)00124-7

Rosi, M., Acocella, V., Cioni, R., Bianco, F., Costa, A., De Martino, P., Giordano, G., Salvatore, I., 2022. Defining the pre-eruptive states of active volcanoes for improving eruption forecasting. Frontiers in Earth Science. https://doi.org/10.3389/feart.2022.795700

Rutarindwa, R., Spiller, E.T., Bevilacqua, A., Bursik, M.I., Patra, A.K., 2019. Dynamic probabilistic hazard mapping in the Long Valley Volcanic Region CA: integrating vent opening maps and statistical surrogates of physical models of pyroclastic density currents. Journal of Geophysical Research: Solid Earth, 124(9), 9600-9621. https://doi.org/10.1029/2019JB017352

Sandri, L., Thouret, J.C., Constantinescu, R., Biass, S., Tonini, R., 2014. Long-term multi-hazard assessment for El Misti volcano (Peru). Bulletin of Volcanology, 76(2), 1-26. https://doi.org/10.1007/s00445-013-0771-9

Sheridan, M.F., Malin, M.C., 1983. Application of computer-assisted mapping to volcanic hazard evaluation of surge eruptions: Vulcano, Lipari, and Vesuvius. Journal of Volcanology and Geothermal Research, 17(1-4), 187-202. https://doi.org/10.1016/0377-0273(83)90067-7

Sieron, K., Capra, L., Rodríguez-Elizararrás, S., 2014. Hazard assessment at San Martín volcano based on geological record, numerical modeling, and spatial analysis. Natural Hazards, 70, 275-297. https://doi.org/10.1007/s11069-013-0807-7

Sieron, K., Ferrés, D., Siebe, C., Constantinescu, R., Capra, L., Connor, C., Connor, L., Groppelli, G., González Zuccolotto, K., 2019. Ceboruco hazard map: part II—modeling volcanic phenomena and construction of the general hazard map. Natural Hazards, 96, 893-933. https://doi.org/10.1007/s11069-019-03577-5

Sieron, K., Juárez Cerrillo, S.F., González-Zuccolotto, K., Córdoba-Montiel, F., Connor, C.B., Connor, L., Tapia-McClung, H., 2021. Morphology and distribution of monogenetic

volcanoes in Los Tuxtlas Volcanic Field, Veracruz, Mexico: implications for hazard assessment. Bulletin of Volcanology, 83(7), 47. https://doi.org/10.1007/s00445-021-01467-y

Sobradelo, R., Martí, J., 2010. Bayesian event tree for long- term volcanic hazard assessment: Application to Teide- Pico Viejo stratovolcanoes, Tenerife, Canary Islands. Journal of Geophysical Research: Solid Earth, 115(B5). https://doi.org/10.1029/2009JB006566

Sofield, D., 1998. History and Hazards of Volcán San Salvador, El Salvador (Doctoral dissertation, Michigan Technological University).

Sofield, D., 2004. Eruptive history and volcanic hazards of Volcan San Salvador. Natural Hazards in El Salvador, 147. https://doi.org/10.1130/0-8137-2375-2.147

Tadini, A., Roche, O., Samaniego, P., Azzaoui, N., Bevilacqua, A., Guillin, A., Gouhier, M., Bernard, B., Aspinall, W., Hidalgo, S., Eychenne, J., de' Michieli Vitturi, M., Neri, A., Cioni, R., Pistolesi, M., Gaunt, E., Vallejo, S., Encalada, M., Yepes, H., Proaño, A., Pique, M., 2021a. Eruption type probability and eruption source parameters at Cotopaxi and Guagua Pichincha volcanoes (Ecuador) with uncertainty quantification. Bulletin of Volcanology, 83(5), 1-25. https://doi.org/10.1007/s00445-021-01458-z

Tadini, A., Bevilacqua, A., Neri, A., Cioni, R., Biagioli, G., de' Michieli Vitturi, M., Esposti Ongaro, T., 2021b. Reproducing pyroclastic density current deposits of the 79 CE eruption of the Somma–Vesuvius volcano using the box-model approach. Solid Earth, 12(1), 119-139. https://doi.org/10.5194/se-12-119-2021

Tadini, A., Azzaoui, N., Roche, O., Samaniego, P., Bernard, B., Bevilacqua, A., Hidalgo, S., Guillin, A., Gouhier, M., 2022. Tephra fallout probabilistic hazard maps for Cotopaxi and Guagua Pichincha volcanoes (Ecuador) with uncertainty quantification. Journal of Geophysical Research: Solid Earth. https://doi.org/10.1029/2021JB022780

Todesco, M., Neri, A., Esposti Ongaro, T., Papale, P., Macedonio, G., Santacroce, R., Longo, A., 2002. Pyroclastic flow hazard assessment at Vesuvius (Italy) by using numerical modeling. I. Large-scale dynamics. Bulletin of Volcanology, 64(3), 155-177. https://doi.org/10.1007/s00445-001-0189-7

Valentine, G.A., Perry, F.V., Connor, C., 2009. Volcanic risk assessment at Yucca Mountain, NV, USA. In: Integration of geophysics, geology, and modeling. Volcanic and Tectonic Hazard Assessment for Nuclear Facilities (Connor, CB, Chapman, NA, Connor, LJ, Eds), Cambridge University Press, Cambridge, 452-480. https://doi.org/10.1017/CBO9780511635380.020

Wadge, G., Isaacs, M.C., 1988. Mapping the volcanic hazards from Soufriere Hills Volcano, Montserrat, West Indies using an image processor. Journal of the Geological Society, 145(4), 541-551. https://doi.org/10.1144/gsjgs.145.4.0541

Wright, H.M., Pallister, J.S., McCausland, W.A., Griswold, J.P., Andreastuti, S., Budianto, A., Primulyana, S., Triastuty, H., 2019. Construction of probabilistic event trees for eruption forecasting at Sinabung volcano, Indonesia 2013–14. Journal of Volcanology and Geothermal Research, 382, 233-252. https://doi.org/10.1016/j.jvolgeores.2018.02.003

Table 1. Input parameters used in numerical simulations of tephra fallout (program TephraProb).

Eruption scenario	**ES1: Plinian**	**ES2: Sub-Plinian**	**ES3: Violent Strombolian**
Vent position	El Boquerón	El Boquerón	Vent opening map ([a])
Number of simulations	1,000	3 x 500	1,000
Seasonality	No	Yes	No
Column height (km above the vent) ([b])	20 - 30	12 – 20	2 – 5
Eruption duration (h) ([c])	1.0 - 24.0	1.0 - 24.0	4.0 – 72.0
Mass (x10^{12} kg) ([c])	0.2 – 5.0	0.05 – 0.5	0.001 – 0.02
Mdϕ ([d])	-1 to -2.5	-1 to -2.5	-6 to -3
$\sigma\phi$ ([d])	2 to 2.5	2 to 2.5	1 to 2
Cell grid dimensions	1.0 km	0.5 km	0.25 km
Reference eruption	G-1	Talpetate I	El Playón and AD 1917 eruptions

([a]) TephraProb simulations were performed using a fixed vent position (at El Playón). Then, the resulting maps of exceedance probability were displaced within the volcanic field and weighted using the vent opening probability maps for small-scale eruptions able to produce fallout deposits presented by Bevilacqua et al. (2021).

([b]) Sampled from a logarithmic PDF.

([c]) Eruption duration is sampled from a uniform PDF. However, following the sampling scheme described by Biass et al. (2016), we also defined a range or variation for erupted mass. When the sampled couple of column height (i.e. eruption rate) and eruption duration gives rise to an erupted mass outside the prescribed range for this parameter, this couple is discarded. Consequently, in practice, sampled eruption durations do not follow a uniform distribution. In fact, most of the values of duration ranges from 2 h to 12 h for ES2, with absence of simulations longer than 21 h. For ES1, most of the simulations are shorter than 12 h.

([d]) Sampled from a uniform probability density function.

Table 2. Input parameters used in numerical simulations of PDCs (programs BoxMapProb 2.0 and ECMapProb 2.0).

Branching box model (BoxMapProb 2.0)		
Eruption scenario	**ES1: Plinian**	**ES2: Sub-Plinian**
Calibration of input parameters	Comparison with reference inundation polygon ([a])	Comparison with reference inundation polygon ([a])
Number of calibration simulations	3 x 900 ([b])	3 x 900 ([b])
Variation range of inputs in calibration simulations ([b])	$V_{0,0} = 10^6 - 10^{11}\ m^3$ $\phi_{0,0} = 0.05 - 0.40$ $w_s = 0.05, 0.30, 1.20\ m/s$ $Fr = 1.1$ $\rho_p = 1500.0\ kg/m^3$ $\rho_g = 1.1\ kg/m^3$	$V_{0,0} = 10^5 - 10^{10}\ m^3$ $\phi_{0,0} = 0.05 - 0.40$ $w_s = 0.05, 0.30, 1.20\ m/s$ $Fr = 1.1$ $\rho_p = 1500.0\ kg/m^3$ $\rho_g = 1.1\ kg/m^3$
Vent in calibration simulations	El Boquerón crater ([c])	NW rim of El Boquerón crater ([c])
Number of calibrated simulations	3 x 3 x 1,000 ([d])	3 x 3 x 1,000 ([d])
Vent in calibrated simulations	Sampled from El Boquerón crater ([e])	Sampled from the rim of El Boquerón crater ([f])
Cell grid dimensions	30 m ([g])	30 m ([g])
Reference eruption	G-1	Talpetate I
Branching energy cone model (ECMapProb 2.0)		
Eruption scenario	**ES2: Sub-Plinian**	**ES3: Violent Strombolian**
Calibration of input parameters	Comparison with reference inundation polygon ([a])	Prescribed distribution of runout distance ([h])
Number of calibration simulations	900	900
Variation range of inputs in calibration simulations ([i])	$H_{0,0} = 100 - 2000\ m$ $tan(\phi) = 0.2 - 1.0$	$H_{0,0} = 100 - 2000\ m$ $tan(\phi) = 0.2 - 1.0$
Vent in calibration simulations	NW rim of El Boquerón crater ([c])	El Playón ([h])
Number of calibrated simulations	3 x 1,000 ([j])	10,000
Vent in calibrated simulations	Sampled from rim of El Boquerón crater ([f])	Sampled following Bevilacqua et al. (2021)
Cell grid dimensions	30 m ([g])	30 m ([g])
Reference eruption	Talpetate I	El Playón and AD 1917 eruptions

([a]) In each set of calibration simulations, we compared each calibration simulation with a reference inundation polygon (G-1 for ES1 and Talpetate I for ES2) considering three comparison metrics: Jaccard index (JI), Hausdorff distance (HD) and root mean square distance (RMSD).

([b]) We performed three sets of 900 calibration simulations associated with three different values of sedimentation velocity (w_s) and fixed values of Froude number (Fr), pyroclast density (ρ_p) and air density (ρ_g). In each set of calibration simulations, the collapsing volume ($V_{0,0}$) and initial concentration of pyroclasts ($\phi_{0,0}$) were sampled within specific variation ranges.

([c]) Assumption based on the characteristics of the reference inundation polygon.

([d]) For each eruption scenario, we developed nine sets of 1,000 calibrated simulations. This derives from the use of three values of sedimentation velocity and three different comparison metrics for the calibration of the model.

([e]) Vent position was sampled uniformly within a 1000-m radius circle located at El Boquerón crater.

([f]) Vent position was sampled uniformly at distances lower than 100 m from the border of a 1000-m radius circle located in El Boquerón crater. This was assumed to reproduce the propagation of PDCs derived from partial collapse processes of the eruptive column, in agreement with the reference PDC considered for this eruption scenario (i.e. Talpetate I).

([g]) SRTM 30 m (Rabus et al., 2003).

([h]) Input parameters were sampled in order to reproduce a prescribed distribution of runout distance (uniform distribution between 1 km and 3 km), for which a set of calibration simulations performed with the vent at El Playon was adopted.

([i]) We performed one set of 900 calibration simulations where the collapse height ($H_{0,0}$) and energy cone slope (ϕ) were sampled within specific variation ranges.

([j]) We developed three sets of 1,000 calibrated simulations. This derives from the use of three different comparison metrics for the calibration of the model.

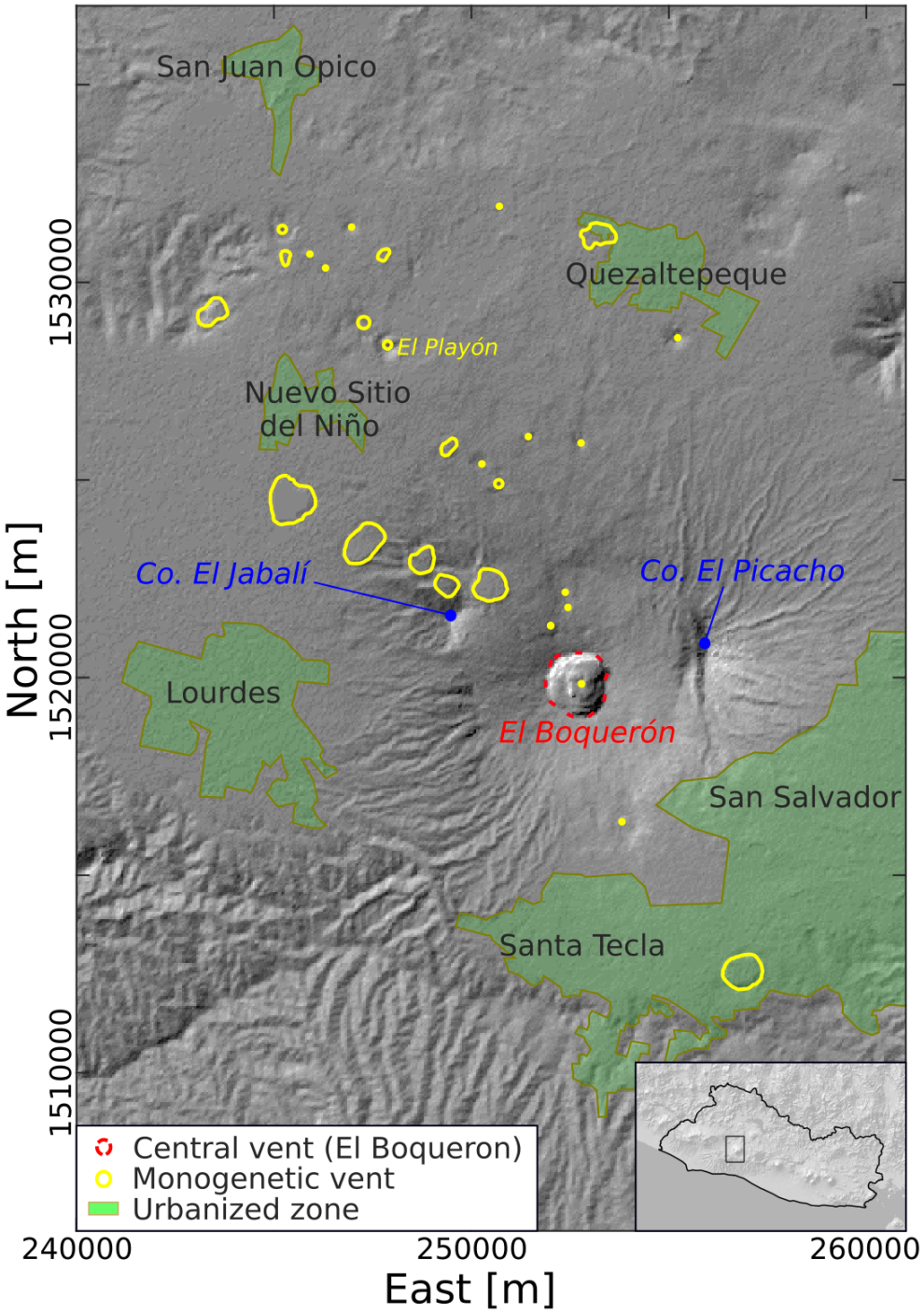

Figure 1. Shaded relief map of San Salvador Volcanic Complex (SSVC). Data of past vents and urbanized zones are also included.

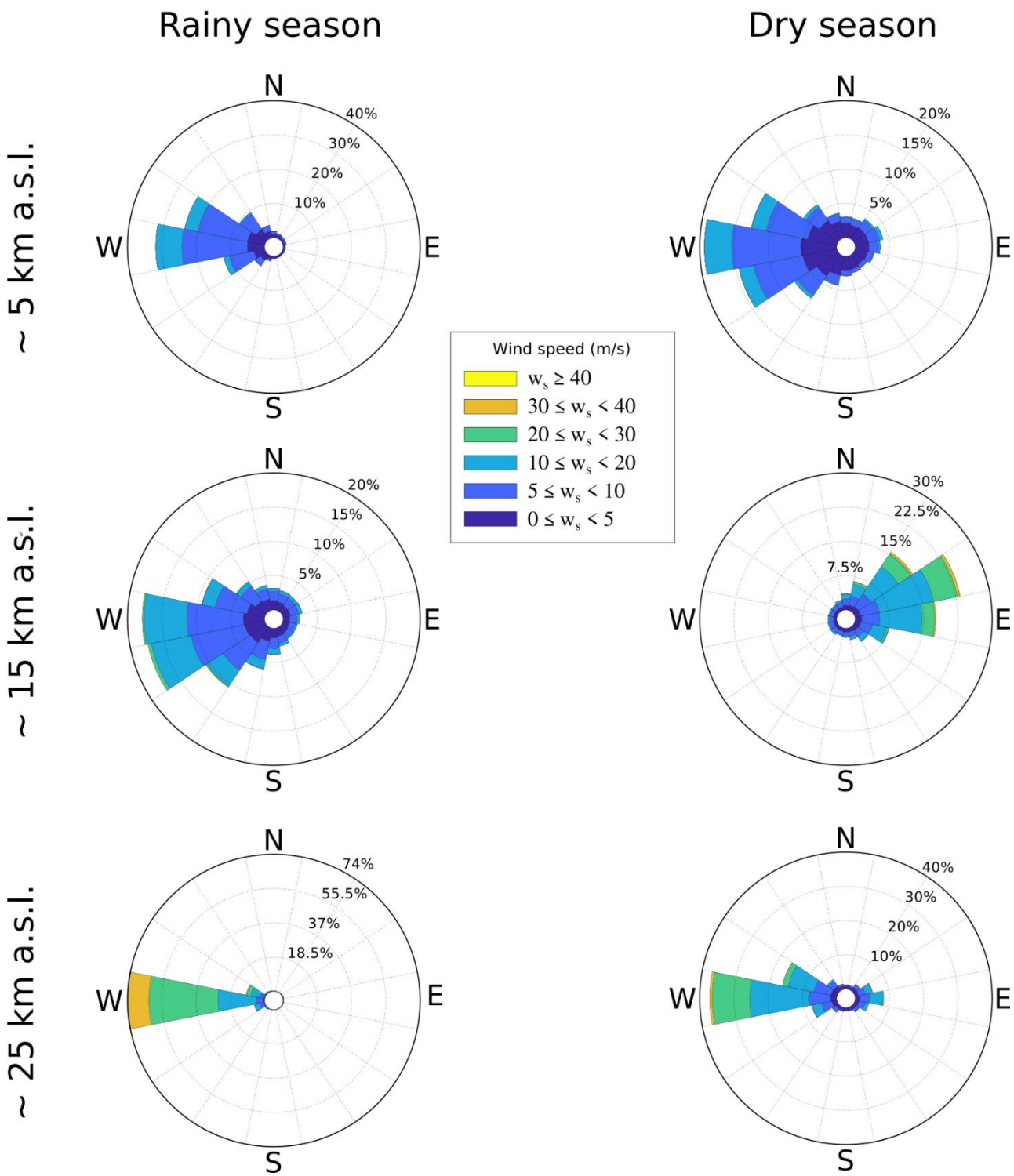

Figure 2. Wind roses at different heights and different seasons at San Salvador Volcanic Complex (SSVC). The rainy season corresponds to the period between July and October and the dry season is the period from November and June. This figure includes data from 2000 to 2020 (NCEP/NCAR Reanalysis database) and shows the frequency of winds blowing to particular directions.

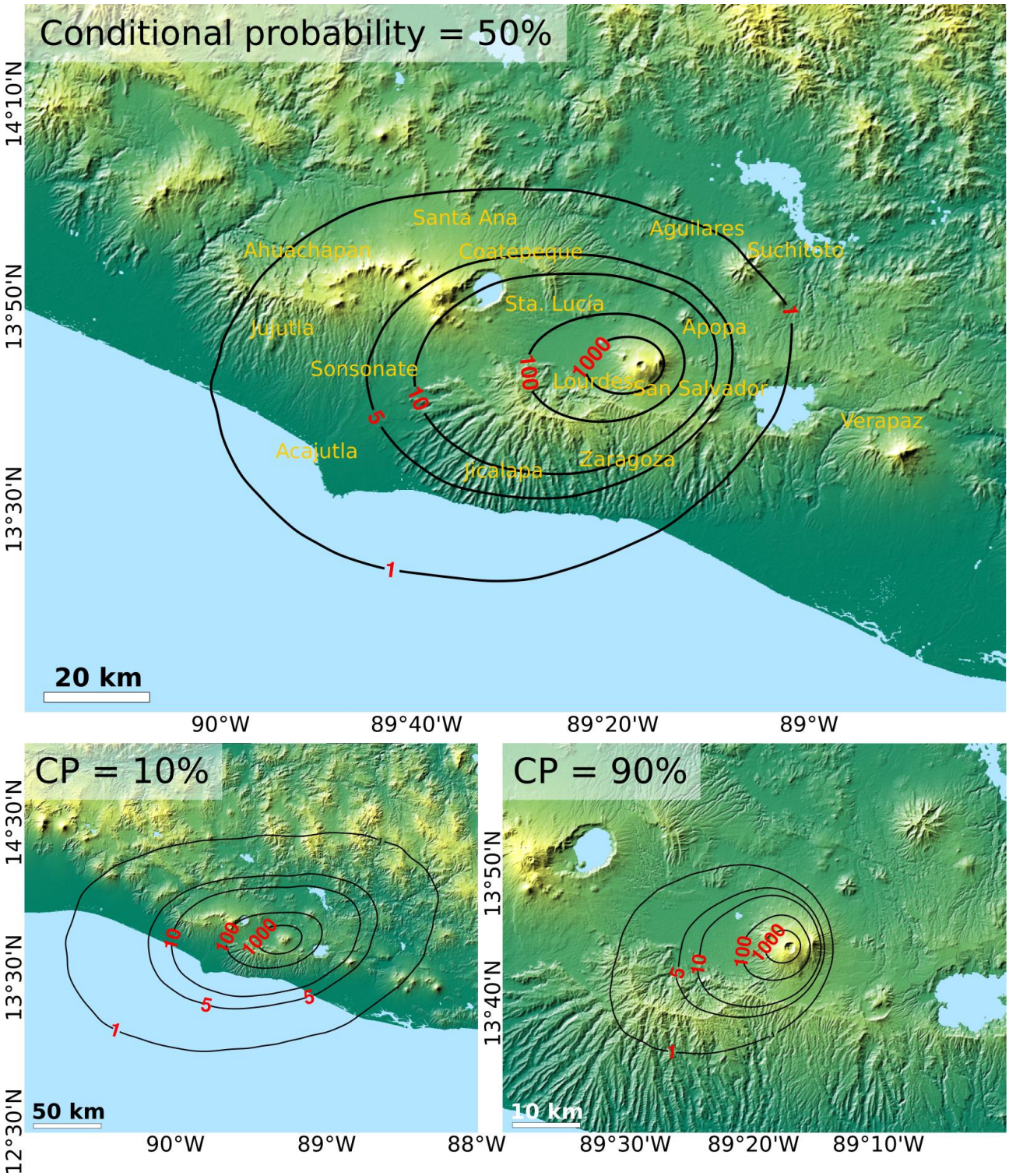

Figure 3. Probabilistic hazard maps of tephra fallout showing a set of isolines of mass per unit area associated with different values of conditional probability (10%, 50%, and 90%) for the occurrence of a Plinian eruption at El Boquerón volcano (plume height between 20 and 30 km). Mass per unit area on the ground is expressed in kg/m^2.

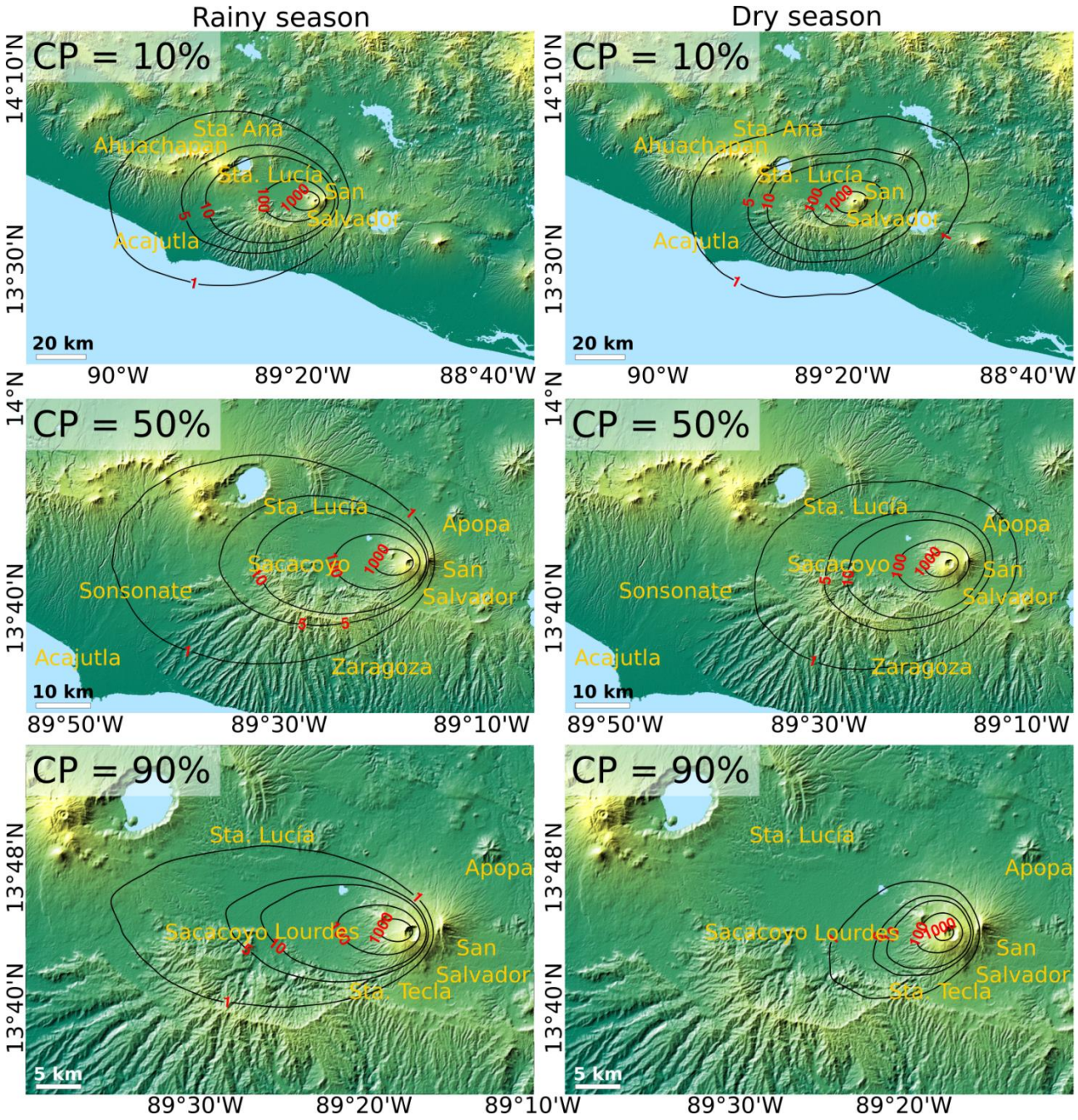

Figure 4. Probabilistic hazard maps of tephra fallout showing a set of isolines of mass per unit area associated with different values of conditional probability (10%, 50%, and 90%) for the occurrence of a sub-Plinian eruption at El Boquerón volcano (plume height between 12 and 20 km). Results are presented separately for the rainy (July - October) and dry (November - June) seasons (the integrated results are presented in Supplementary Figure S3). Mass per unit area on the ground is expressed in kg/m^2.

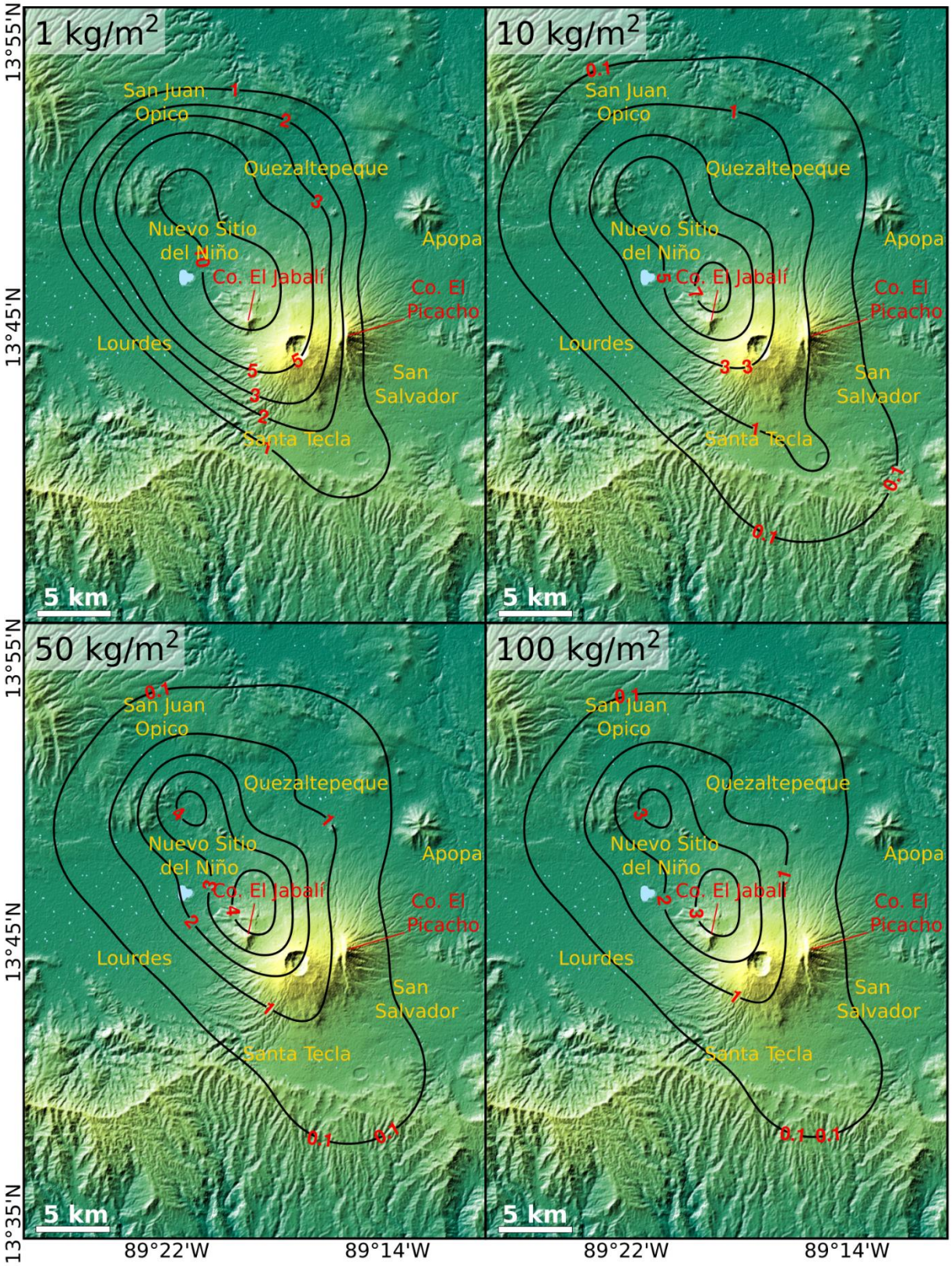

Figure 5. Probabilistic hazard maps of tephra fallout showing a set of isolines of exceedance probability associated with different values of mass per unit area on the ground (10, 50, 100 and 1000 kg/m^2). These values are conditioned on the occurrence of a violent Strombolian eruption at SSVC (plume height between 2 and 5 km). Exceedance probabilities are expressed in percent.

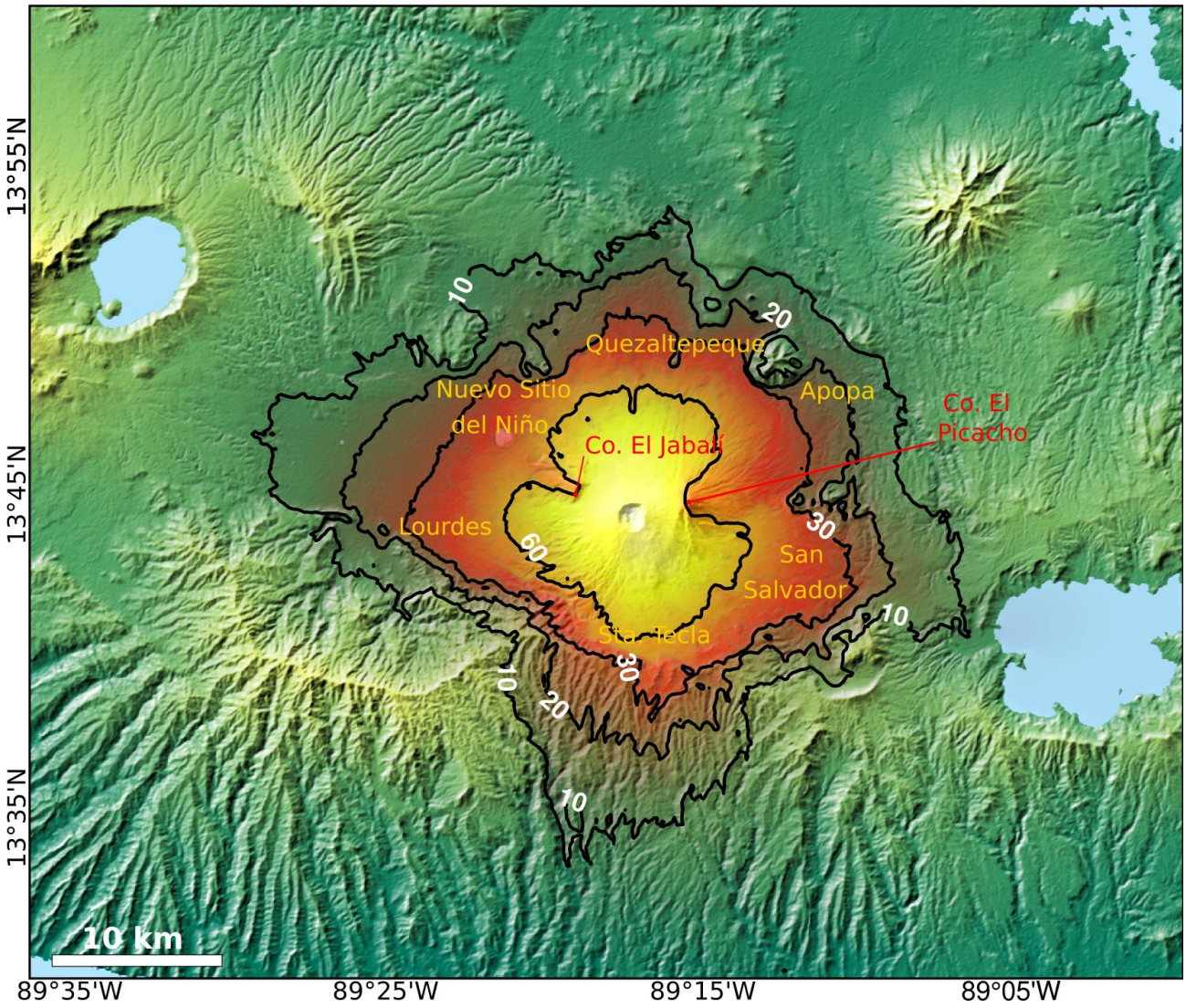

Figure 6. Conservative probabilistic hazard map of PDC (see text for explanation) showing the inundation probability conditioned on the occurrence of a column collapse during a Plinian eruption (reference event: G-1) at El Boquerón volcano. This map was computed using the branching box model. In order to produce conservative results, for each pixel, we present the maximum PDC inundation probability among three maps (Supplementary Figure S4), which are defined as the average inundation probability derived from the use of three different comparison metrics for the model calibration (JI, HD and RMSD, see main text and Table 2), considering different values of sedimentation velocity. The input parameters of our numerical simulations were sampled using a set of calibration procedures presented in Aravena et al. (2022). Results are expressed in percent.

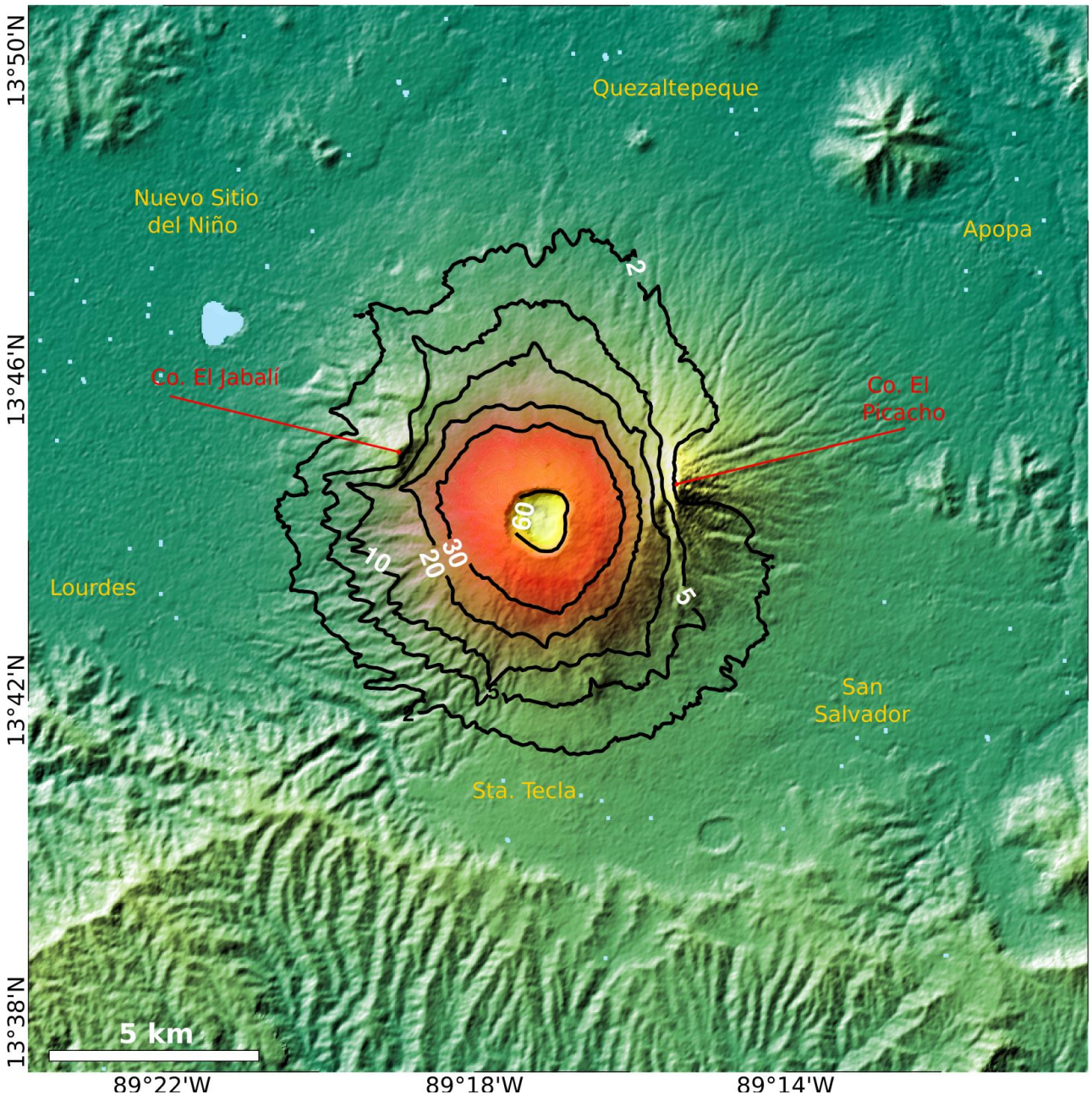

Figure 7. Conservative probabilistic hazard map of PDC showing the inundation probability conditioned on the occurrence of partial column collapse during a sub-Plinian eruption (reference event: Talpetate I) at El Boquerón volcano. This map was computed using the branching box model and the branching energy cone model. In order to produce conservative results, for each pixel, we present the maximum PDC inundation probability among four maps (Supplementary Figures S5 and S7). Three of them were calculated using the branching box model and are defined as the average inundation probability derived from the use of three different comparison metrics for the model calibration (JI, HD and RMSD, see main text and Table 2), considering different values of sedimentation velocity. The other map was calculated using the branching energy cone model and is defined as the average inundation probability derived from the application of three different comparison metrics for the model calibration as well (JI, HD and RMSD, see main text and Table 2). The input parameters of our numerical simulations were sampled using a set of calibration procedures presented in Aravena et al. (2022). Results are expressed in percent.

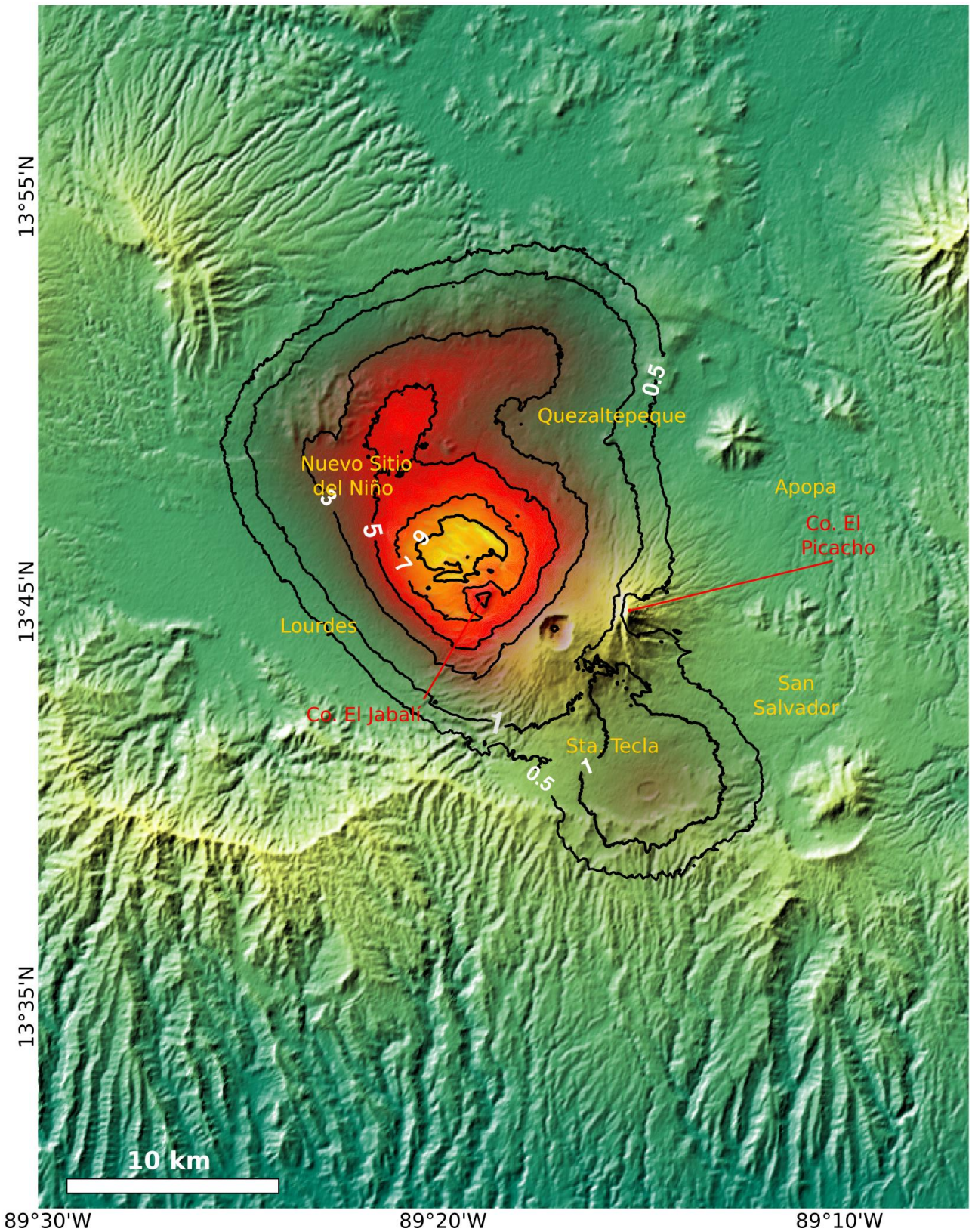

Figure 8. Probabilistic hazard map of PDC showing the inundation probability conditioned on the occurrence of a small-scale PDC at the SSVC. Inundation probabilities are expressed in percent.